High Proton Conductivity in a Flexible, Cross-Linked, Ultramicroporous Magnesium Tetraphosphonate Hybrid Framework

13 AUTHORS, INCLUDING:

High Proton Conductivity in a Flexible, Cross-Linked, Ultramicroporous Magnesium Tetraphosphonate Hybrid Framework

Rosario M. P. Colodrero,[†] Pascual Olivera-Pastor,[†] Enrique R. Losilla,[†] Daniel Hernández-Alonso,[†] Miguel A. G. Aranda,[†] Laura Leon-Reina,[‡] Jordi Rius,[§] Konstantinos D. Demadis,[‖] Bernard Moreau,[⊥] Didier Villemin,[⊥] Miguel Palomino,[#] Fernando Rey,[#] and Aurelio Cabeza*,[†]

[†]Departamento de Química Inorgánica, Universidad de Málaga, Campus Teatinos s/n, 29071-Málaga, Spain

[‡]Servicios Centrales de Apoyo a la Investigación, Universidad de Málaga, Campus Teatinos s/n, Málaga-29071, Spain

[§]Institut de Ciència de Materials de Barcelona, 08193 Bellaterra, Catalunya, Spain

[‖]Crystal Engineering, Growth and Design Laboratory, Department of Chemistry, University of Crete, Voutes Campus, Crete, GR-71003, Greece

[⊥]Laboratoire de Chimie Moléculaire et Thioorganique, UMR CNRS 6507, INC3M, FR 3038, ENSICAEN & Université de Caen, Caen, France

[#]Instituto de Tecnología Química (UPV-CSIC), Avenida de los Naranjos s/n, 46022, Valencia, Spain

Ⓢ Supporting Information

ABSTRACT: Multifunctional materials, especially those combining two or more properties of interest, are attracting immense attention due to their potential applications. MOFs, metal organic frameworks, can be regarded as multifunctional materials if they show another useful property in addition to the adsorption behavior. Here, we report a new multifunctional light hybrid, $MgH_6ODTMP \cdot 2H_2O(DMF)_{0.5}$ (**1**), which has been synthesized using the tetraphosphonic acid H_8ODTMP, octamethylenediamine-N,N,N',N'-tetrakis(methylenephosphonic acid), by high-throughput methodology. Its crystal structure, solved by Patterson-function direct methods from synchrotron powder X-ray diffraction, was characterized by a 3D pillared open framework containing cross-linked 1D channels filled with water and DMF. Upon H_2O and DMF removal and subsequent rehydration, $MgH_6ODTMP \cdot 2H_2O$ (**2**) and $MgH_6ODTMP \cdot 6H_2O$ (**3**) can be formed. These processes take place through crystalline−quasi-amorphous−crystalline transformations, during which the integrity of the framework is maintained. A water adsorption study, at constant temperature, showed that this magnesium tetraphosphonate hybrid reversibly equilibrates its lattice water content as a function of the water partial pressure. Combination of the structural study and gas adsorption characterization (N_2, CO_2, and CH_4) indicates an ultramicroporous framework. High-pressure CO_2 adsorption data are also reported. Finally, impedance data indicates that **3** has high proton conductivity $\sigma = 1.6 \times 10^{-3}$ S cm^{-1} at $T = 292$ K at ∼100% relative humidity with an activation energy of 0.31 eV.
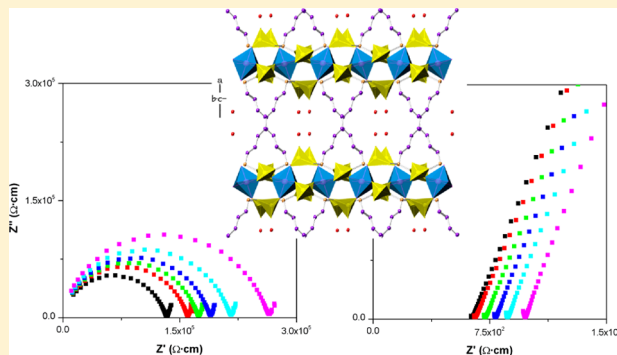
■ INTRODUCTION

Design of inorganic−organic hybrid compounds for specific applications is a major challenge in metal organic framework (MOF) synthesis, and hence, new synthetic strategies are continuously being investigated. Current interest is focused on developing new porous framework materials with potential applications in gas storage, separation, and catalysis.[1−3] Appropriate selection of the organic linker, metal ion, and method of preparation have yielded to new hybrid porous materials possessing variable structural flexibility. On the other hand, high porosity and high surface area, together with permanent pore size and pore shape, are attractive properties for gas storage application. Among the possible applications, trapping gases of environmental significance, like CO_2 or CH_4,

is now recognized as being of paramount importance.[4] For this purpose, materials with low framework density are also desirable. As a component of porous coordination polymer materials, magnesium is an excellent candidate because it is a light metal ion with coordinative properties similar to those of various divalent metal ions of the first transition series, particularly Zn^{2+}. In fact, Mg/DOBDC (DOBDC = dioxybenzenedicarboxylate) with coordinatively unsaturated metal sites (CUS) was reported to be a highly competitive material in CO_2 capture.[3i,j] However, so far, only a few cases of magnesium-containing MOFs have been reported.[3,5−7] A chiral

open-framework magnesium-based MOF showing selective H_2 adsorption and CO_2 uptake has been recently reported.[5]

Applications of MOFs as ion conductors have not been explored as broadly as gas storage, in spite of the important role that proton (ion) conductivity in solid-state materials may play due to their potential applications in transport dynamics, electrochemical devices, and/or fuel cells.[8] Proton conductivity requires proton carriers such as H_3O^+ or H^+, with the involvement of acidic moieties, whereas conducting pathways are usually based on hydrogen-bonded networks for ion conduction. To date, only a few works related to proton conductivity of MOFs have been reported,[8−10] some of them with values of proton conductivity as high as 1.1×10^{-3} S cm^{-1} at room temperature.[10]

Compared to carboxylate-based MOFs, metal phosphonates fulfilling all of the MOFs characteristics are considerably scarce in the literature, because they tend to form densely packed layered structures that are not porous. Conversely, a different set of metal phosphonates may exhibit permanent porosity, albeit with poorly crystalline frameworks (coined as unconventional MOFs or UMOFs).[11,12] However, issues related to low crystallinity and/or porosity may be, at least partially, circumvented by the use of polyfunctional and/or polyphosphonic ligands. Thus, new building blocks may lead to new phosphonate-based MOFs with attractive properties.[11] Aminomethylenephosphonic acids belong to this group of versatile organic linkers providing a complete set of new compounds with different topologies and interesting properties,as a result of the different connectivity between the organic moieties and the metallic centers.[13]

Extending previous work on CaH$_6$DTMP, [H$_8$HDTMP = h e x a m e t h y l e n e d i a m i n e - N,N,N',N' - t e t r a k i s - (methylenephosphonic acid)], an adsorbate-responsive material with 2D topology exhibiting a "breathing" phenomenon,[14] and La(H$_5$HDTMP)·7H$_2$O,[15] a 3D ultramicroporous material with high proton conductivity, here we report the synthesis, crystal structure, adsorption behavior, and proton conductivity properties of a flexible Mg hybrid material using as linker the o c t a m e t h y l e n e d i a m i n e - N,N,N',N' - t e t r a k i s - (methylenephosphonic acid), [H$_8$ODTMP].

■ EXPERIMENTAL SECTION

General Information. All water-soluble metal salts were commercial samples and used without further purification. H$_8$ODTMP was synthesized according to literature procedures.[16] Stock solutions of HNO$_3$ or NH$_3$ were used for pH adjustments. In-house, deionized (DI) water was used for all syntheses. Elemental analyses (C, H, N) were measured on a Perkin−Elmer 240 analyzer. Thermogravimetric analysis (TGA) data were recorded on an SDT-Q600 analyzer from TA Instruments. The temperature was varied from room temperature to 1000 °C at a heating rate of 10 °C·min^{-1}. Measurements were carried out on samples in open platinum crucibles under air flow.

Low-Scale High-Throughput Study. Synthesis conditions were screened by a high-throughput methodology with a syste, and initial experimental conditions previously reported.[17] The aluminum autoclave block contains 6 Teflon-lined reaction chambers of 5 mL volume. Hydro/solvothermal reactions of H$_8$ODTMP acid with Mg^{2+} salt were carried out in H$_2$O/DMF mixtures (molar ratios 2:0, 2:1, and 2:2). The reaction mixture was prepared by mixing a 0.115 M aqueous solution of Mg(NO$_3$)$_2$·6H$_2$O with H$_8$ODTMP acid, as a solid, or as 0.115 M aqueous solution. In this latter case, H$_8$ODTMP was dissolved by adding dropwise a 1 M aqueous solution of NH$_3$ to a suspension of the solid product in 10 mL of DI water up to a clear solution, pH ≈ 2.5. For the syntheses in water, 1:2, 1:1, 2:1, and 4:1

Mg:H$_8$ODTMP molar ratios and initial pH values of 1.0, 2.0, 2.5, 3.5, and 4.5 were tested. For the syntheses in H$_2$O/DMF, 1:1 and 2:1 Mg:H$_8$ODTMP molar ratios were studied and the pH values were those of the mixtures, 3.1 and 2.1, respectively (just given as an indication). A total filling volume of ∼3 mL per reactor was used. The reaction block was heated to 130 °C for 2 days. The reaction products were filtered off, washed with water, and dried at 50 °C.

Large-Scale Synthesis. MgH$_6$ODTMP·2H$_2$O·(DMF)$_{0.5}$ (**1**) was prepared by dissolving Mg(NO$_3$)$_2$·6H$_2$O (0.384 mmol, 96.6 mg) in 3.35 mL of DI under stirring. A 6.70 mL amount of DMF was added to this solution while maintaining stirring, followed by 200 mg of solid H$_8$ODTMP (0.384 mmol). The pH of the resulting solution was 3.2. The reaction was conducted at 130 °C for 7 days in a Teflon-lined autoclave with a volume of 45 mL. The resulting solid was filtered off, washed twice with DI and acetone, and dried at 50 °C. Anal. Calcd for **1**, MgP$_4$O$_{12}$N$_2$C$_{12}$H$_{30}$·2H$_2$O·0.5DMF: C, 26.36; H, 6.15; N, 5.69. Found: C, 26.47; H, 6.08; N, 5.86. Yield ≈ 60% based on the metal.

MgH$_6$ODTMP·2H$_2$O (**2**) was prepared by heating **1** at 423 K for 4 h. Anal. Calcd for **2**, MgP$_4$O$_{12}$N$_2$C$_{12}$H$_{30}$·2H$_2$O: C, 24.91; H, 5.93; N, 4.84. Found: C, 24.37; H, 5.87; N, 5.07.

Structural Characterization. Laboratory X-ray powder diffraction (XRPD) patterns were collected on a PANanalytical X'Pert Pro diffractometer equipped with an X'Celerator detector. XRPD patterns corresponding to the single phases were autoindexed using the DICVOL06 program,[18] and space groups were derived from the observed systematic extinctions. The crystal structure of **1** was successfully solved following an ab initio methodology. For this purpose, a high-resolution synchrotron powder data set was collected on ID31 powder diffractometer of ESRF, European Synchrotron Radiation Facility (Grenoble, France), using a wavelength $\lambda = 0.2998$ Å selected with a double-crystal Si (111) monochromator and calibrated with Si NIST ($a = 5.43094$ Å). The Debye−Scherrer configuration was used with the sample loaded in a rotating borosilicate glass capillary of diameter of 1.0 mm. The overall measuring time was ∼100 min to have very good statistics over the angular range 1.7−16° (in 2θ). Data from the multianalyzer Si(111) stage were normalized and summed into 0.003° step size with local software. The integrated intensities extracted with the program Ajust[19] were introduced in the direct methods program XLENS.[20] The starting framework model, containing all atoms in the asymmetric part of the unit cell except those corresponding to the solvent, was derived from interpretation of the electron density map computed with the set of refined phases with the highest combined figure of merit. The crystal structure was refined by the Rietveld method[21] using the GSAS package[22] and the EXPGUI graphic interface.[23] The following soft constraints were imposed in order to preserve chemically reasonable geometries for the phosphonate, alkyl chain, and amine groups. The soft constrains were as follows: /PO$_3$C tetrahedron/P−O (1.53(1) Å), P−C (1.80(1) Å), O···O (2.55(2) Å), O···C (2.73(2) Å), /N(CH$_2$)$_3$ amine group/N−C (1.50(1) Å), C···C (2.45(2) Å) and/alkyl chain/ C−C (1.50(1) Å), C$_{chain}$···C$_{chain}$ (2.50(2) Å). No attempts to locate the H atoms were carried out due to the limited quality of the XRPD data. An isotropic atomic displacement parameter was fixed for all atoms. Details for data collection and refinement are included in the CIF file in the Supporting Information, and the final Rietveld plot is given in the Supporting Information as Figure S1.

An initial thermodiffractometric study was carried out for the sample loaded in an Anton Paar HTK1200N Camera under static air. Data were collected at different temperature intervals from room temperature up to 493 K with a heating rate of 5 K·min^{-1} and a delay time of 10 min to ensure thermal stabilization. The data acquisition range was 4−50° (2θ) with a step size of 0.033° and an equivalent counting time of 250 s/step. A second thermodiffractometric study was carried out in the same camera but under vacuum, ∼2.5 × 10^{-4} bar. Patterns were also collected at different temperatures from room temperature to 423 K at the same heating rate, stabilization time, and measurement conditions as describe above.

Gas Sorption Measurements. The N$_2$ adsorption−desorption isotherms for **1** were measured in a Micromeritic ASAP 2020 apparatus. The sample was degassed under high vacuum, ∼5 × 10^{-6}

Table 1. Selected Crystallographic Data for Magnesium Tetraphosphonate Hybrid Materials from Laboratory Powder X-ray Diffraction

	1	2	3
empirical formula	$MgP_4O_{14.5}N_{2.5}C_{13.5}H_{37.5}$	$MgP_4O_{14}N_2C_{12}H_{34}$	$MgP_4O_{18}N_2C_{12}H_{42}$
extended formula	$MgH_6ODTMP \cdot 2H_2O(DMF)_{0.5}$	$MgH_6ODTMP \cdot 2H_2O$	$MgH_6ODTMP \cdot 6H_2O$
fw (g·mol^{-1})	615.15	578.60	650.6
Space group	$C2/c$	$C2/c$	$C2/c$
a (Å)	29.654	28.785	28.835
b (Å)	8.622	8.642	8.615
c (Å)	9.704	9.671	9.651
α (deg)	90.0	90.0	90.0
β (deg)	95.49	94.40	94.41
γ (deg)	90.0	90.0	90.0
V (Å^3)	2469.7	2398.8	2390.5
M20	29	17	11
F20	79 (0.003, 74)	34 (0.006, 105)	19 (0.009, 121)
Z	4	4	4
ρ_{calcd} (g·cm^{-3})	1.66	1.60	1.78
V (Å^3/atom-non-H)	17.32	18.17	16.44

bar, at 423 K for 12 h, and the measured weight loss showed full removal of the solvents. The N_2 isotherms, obtained at 77 K, were analyzed by the Brunauer−Emmett−Teller (BET) method. The CO_2 adsorption isotherm for degassed **1** was obtained at 273 K and analyzed by the Dubinin−Radushkevich (DR) method.[24]

Low-pressure CO_2 and CH_4 isotherms (up to 100 kPa) were measured at different temperatures (273, 283, 293, 303, and 318 K) in a Micromeritics ASAP 2010 volumetric instrument in order to get more reliable data in the low-pressure range. Temperature was controlled by means of a thermostatic Julabo F32-HL bath. CO_2 and CH_4 adsorption data at different temperatures were fitted by the Virial equation[25] for calculating the corresponding isosteric heat of adsorption (q_{st}) by applying the Clausius−Clapeyron equation.[26]

Also, the high-pressure CO_2 isotherm (up to 900 kPa) was measured at 303 K on an IGA-3 gravimetric instrument from Hiden Isochema Ltd. equipped with a thermostatic bath FP50-HE from Julabo.

Conductivity Characterization. Electrical characterization for Mg hybrid using **3** as starting material was carried out on a cylindrical pellet (∼10 mm of diameter and ∼2 mm of thickness) obtained by pressing ∼0.2 g of sample at 1000 MPa for 2 min. The pellet was pressed between porous C electrodes (Sigracet, GDL 10 BB, no Pt). Impedance spectroscopy data were collected using a HP4284A impedance analyzer over the frequency range from 20 Hz to 1 MHz with an applied voltage of 0.2 V (for a relative humidity of 82%, the sample was very resistive and so the applied voltage was increased to 1 V). Electrical measurements, controlled by the winDETA package of programs,[27] were taken from 292 to 282 K in 2 K steps in a closed gas thermostatized cell with a thermocouple next to the pellet. The relative humidity (RH) was obtained by a continuous flow of water-saturated air through the cell. Air was bubbled in a thermostatic Julabo F32 water bath at different temperatures with a precision of 0.1 K. The pellet was equilibrated at a given RH for 2 h to ensure a fixed water content of the sample. RH is approximately constant in the narrow measured temperature range of 10 K.

RESULTS AND DISCUSSION

Syntheses. In contrast to other metal tetraphosphonates,[14,15] crystallization at room temperature from aqueous solution of Mg^{2+} salt with H_8ODTMP was unsuccessful as no solid was formed. The high-throughput screening of the system $Mg^{2+}/H_8ODTMP/H_2O$ did not reveal any solid at 130 °C by hydrothermal reaction for 4:1 and 1:1 $Mg:H_8ODTMP$ molar ratios in the studied pH range, 1.0−4.5. A solid of low crystallinity was obtained for 1:2 $Mg:H_8ODTMP$ molar ratio

and pH < 2.5. Solvothermal syntheses in H_2O/DMF mixtures using 2:1 and 1:1 $Mg:H_8ODTMP$ molar ratios and maintaining the pH unchanged at 3.1 led to a crystalline single-phase compound with the following stoichiometry, $MgH_6ODTMP \cdot 2H_2O(DMF)_{0.5}$ (**1**). The beneficial influence of DMF in the crystallization of the compound may be due not only to lowering the solubility but also to a structure-directing agent effect; in fact, a small amount of DMF still remains in the as-synthesized material, **1**. The powder pattern of **1** was autoindexed, and selected crystallographic details are given in Table 1. Syntheses without DMF invariably gave Mg hybrid compounds with lower crystallinity. Synthesis in water with a 1:2 $Mg:H_8ODTMP$ molar ratio and pH = 3.5 gave the solid with sharper diffraction peaks of this series. The framework of this compound must be the same as that of **1**, as the shapes of the powder patterns were quite similar, and the stoichiometry should be close to $MgH_6ODTMP \cdot nH_2O$ ($n \approx 4$). This series, DMF free, was not further studied because of their broad powder diffraction patterns.

Thermal Behavior and Water Content. The TGA curve for **1** is displayed in Figure 1. There are three consecutive mass
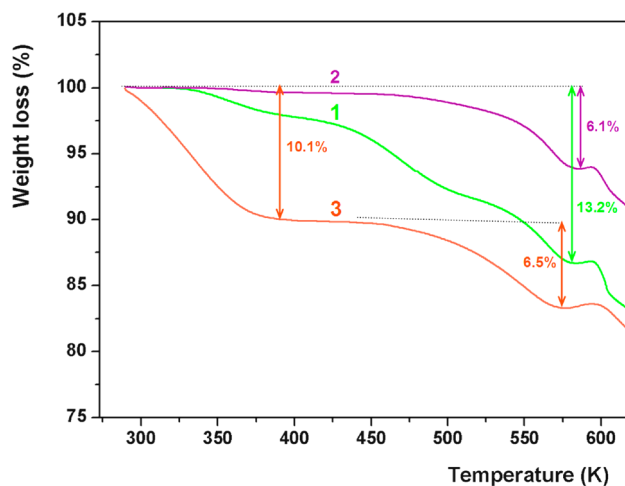

Figure 1. Thermogravimetric analysis curves for **1** [$MgH_6ODTMP \cdot 2H_2O(DMF)_{0.5}$], **2** [$MgH_6ODTMP \cdot 2H_2O$], and **3** [$MgH_6ODTMP \cdot 6H_2O$].
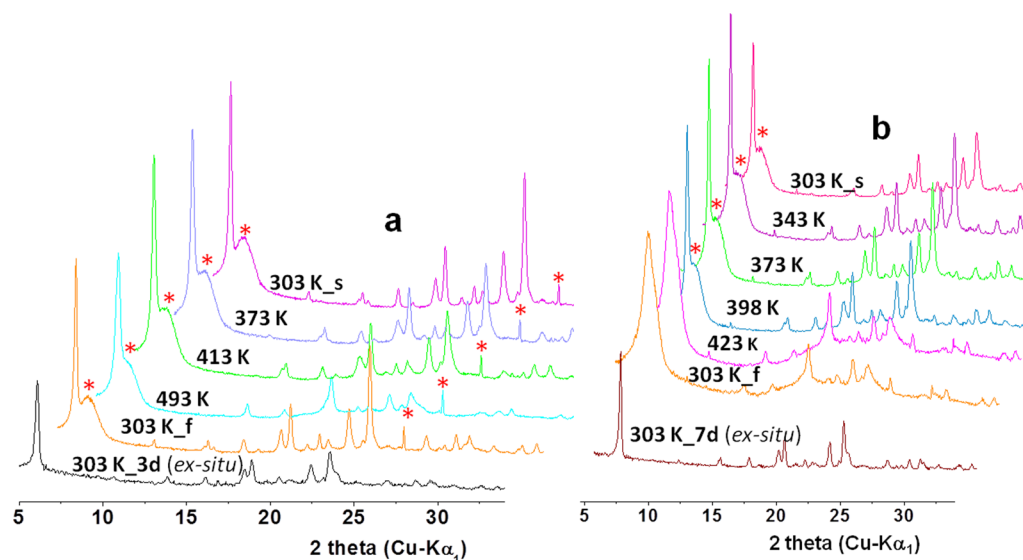
Figure 2. Thermodiffractometric study for **1**. (a) Variable-*T* powder diffraction data under room pressure together with the ex-situ pattern of the final rehydrated compound after 3 days. (b) Variable-*T* data under low pressure, ∼2.5 × 10^{-4} bar, together with the ex-situ pattern of final rehydrated compound after 7 days, **3**. Stars highlight peaks coming from the chamber.

losses up to 563 K followed by a very small plateau. These weight losses correspond to removal of the DMF and water (experimental 13.2%, calculated for 0.5 DMF and 2 H_2O molecules, 11.8%). At higher temperatures, the organic moiety is decomposed and finally there is a significant weight loss close to 1100 K, which is likely related to P_2O_5 release. The final thermal decomposition crystalline products were $Mg_2P_4O_{12}$ (PDF 01-070-1803) and $Mg(PO_3)_2$ (PDF 00-027-1273). The overall measured weight loss up to 1273 K, 65.2%, agrees fairly well with the calculated loss, 66.9%, for the following mixture: 1/2 of $Mg_2P_4O_{12}$ and 1 of $Mg(PO_3)_2$.

The dehydration process of **1** was also followed by thermodiffractometry. Figure 2a shows the variable-*T* powder patterns under room pressure at open atmosphere. As the thermal behavior of the guest species is a key issue in this work, a second study was carried out under vacuum to highlight possible differences. Hence, Figure 2b shows the variable-*T* powder patterns obtained in a closed chamber under vacuum, ∼2.5 × 10^{-4} bar. As can be seen, the sample heated at 423 K under vacuum, Figure 2b, undergoes a partial amorphization which was evident by a strong increase in the background intensity and also by a broadening of the diffraction peaks. In these conditions, full removal of the guest species (DMF and water) takes place.

On the other hand, heating **1** under open atmosphere showed a more robust behavior, see Figure 2a. For instance, **1** heated to at 413 K under open atmosphere is not amorphous, see Figure 2a, but heated at 423 K under vacuum is partly amorphsized, see Figure 2b. The sample composition heated at 413 K under open atmosphere was determined to be $MgH_6ODTMP\cdot2H_2O$, **2**, see below. Amorphization at room pressure starts close to 493 K. Upon cooling under open atmosphere, the compound partially recovers its crystallinity. In these conditions, partial rehydration takes place very rapidly, with two water molecules being taken within minutes. Figure 2a also shows the ex situ powder pattern of the sample rehydrated after 3 days for the sake of comparison. Furthermore, these structural changes upon water uptake are much more evident

when dealing with the product obtained under vacuum, where full crystallinity is recovered, see Figure 2b.

$MgH_6ODTMP\cdot2H_2O$, **2**, was obtained by heating **1** at 423 K for 4 h, and chemical analysis is given in the Experimental Section. The powder pattern of **2** was autoindexed, and the results are also given in Table 1. It must be highlighted that **2** readsorbs additional water to yield a stoichiometry close to 4.5 water molecules. This process occurs rapidly, in about 2 h at open atmosphere. On the other hand, the stoichiometry of the quasi-amorphous material obtained in situ by heating **1** at 413 K under vacuum for 12 h very likely corresponds to anhydrous MgH_6ODTMP. Rehydration of this sample at room temperature for 7 days, under the humidity of a saturated NaCl solution, resulted in the highly hydrated material, $MgH_6ODTMP\cdot6H_2O$, **3**. The powder pattern of this solid reveals a highly crystalline material, see Figure 2b, and the indexing result is also shown in Table 1.

Therefore, **1** undergoes a crystalline−amorphous−crystalline change under heating−cooling−rehydrating conditions. This transformation cannot be regarded as strictly reversible because the guest contents of the starting, **1**, and final, **3**, compounds are not the same. However, the integrity of the guest-responsive framework is maintained intact, as shown by powder diffraction, see Figure 2 and Table 1.

TG analysis curves for **2** and **3** are also shown in Figure 1. The TGA curve for **2** shows a water mass loss in a single step. The measured water loss, 6.1%, agrees quite well with the calculated one, 6.22%. On the other hand, the TGA curve for **3** shows a mass loss in two steps. The first one, from room temperature to ∼400 K, is associated to the weight loss of ∼4 lattice waters (exp 10.1%, calcd 11.07%). The second weight loss appears between 450 and 550 K, corresponding to loss of the remaining 2 lattice waters (exp 6.5%, calcd 5.53%). The overall measured weight loss for **3** up to 550 K, 16.6%, agrees very well with the calculated value for six water molecules, 16.60%.

From the discussion given above, it is clear that the water content of $MgH_6ODTMP\cdot nH_2O$ varies with temperature. However, at a fixed temperature, open-framework solids may

equilibrate their water contents to the external water partial pressure. To investigate this behavior, with implications for the proton conductivity study reported below, a water adsorption study was designed within the thermal analyzer instrument. First, **1** was heated up to 500 K and held for 15 min under a continuous flow of N_2 gas to ensure full water and DMF removal, see Figure 3 (left). Then the anhydrous sample was in
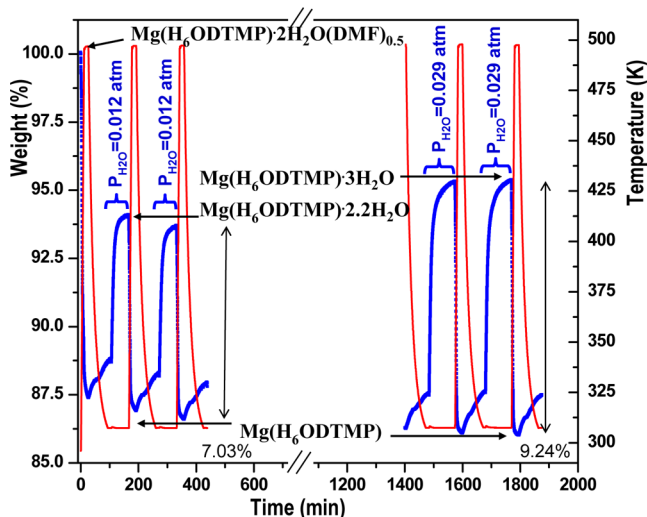

Figure 3. Water adsorption measurements at two different water partial pressures, 0.012 (left) and 0.029 atm (right), and at a fixed temperature of 308 K. TGA loss/gain curve is shown in blue (left y axis). Temperature profile is shown in red (right y axis). Starting sample, **1**, was heated at 500 K for 15 min to ensure full guest species removal. Different water contents are displayed to highlight the ability of the framework to uptake/remove lattice water as a function of the external water partial pressure (or relative humidity).

situ cooled at 308 K. Second, MgH_6ODTMP was exposed to a wet N_2 flow of $p(H_2O) = 0.012$ atm, which was obtained by bubbling within a water bath thermostatized at 288 K, for 60 min. Under this gas flow and at a fixed sample temperature of 308 K, MgH_6ODTMP gains weight, see Figure 3 (left). In the thermal analyzer chamber the RH was 21.8% and the water uptake, 7.03 wt %, corresponds to $n = 2.18$, i.e., $MgH_6ODTMP·2.18H_2O$. Water removal on heating under N_2 flow and subsequent water uptake in the second cycle is reversible. It must be highlighted that for anhydrous MgH_6ODTMP the thermogravimmetric baseline under N_2 flow is not constant and there is a small weight gain, see Figure 3, likely due to water uptake from the continuous flow of N_2 which contains 2 ppm of water. Third, at the same constant sample temperature of 308 K anhydrous MgH_6ODTMP was exposed for 90 min to wet N_2 flow with a higher water partial pressure, $p(H_2O) = 0.029$ atm, obtained by thermostatizing the bath at 298 K. As expected, at a larger RH value, 40.5%, the measured water uptake was larger, 9.24 wt %, which corresponds to $MgH_6ODTMP·2.93H_2O$, see Figure 3 (right). Subsequent water removal on heating and water uptake in the second cycle were fully reversible. Therefore, this experiment showed that the Mg hybrid, at a fixed temperature of 308 K, reversibly equilibrates to a water content of $MgH_6ODTMP·2.18H_2O$ and $MgH_6ODTMP·2.93H_2O$ for water partial pressures of 0.012 and 0.029 atm, respectively.

To better understand the water content variation of **3** with temperature a second water adsorption/desorption experiment

was carried out. In this case, **3** was exposed to repeated cycles of heating and cooling under a constant water-saturated N_2 flow between room temperature and 383 K. As shown in Figure S2 (Supporting Information), ~3.5 lattice waters were lost upon the first heating, whereas ~2.5 lattice waters were recovered by subsequent cooling. A second cycle shows a fully reversible water release and uptake on heating and cooling, respectively. Thus, the final hydration degree of the solid in these experimental conditions was $MgH_6ODTMP·5H_2O$.

Crystal Structure. Compound **1** crystallizes in the monoclinic system, $C2/c$ space group, and a cell volume of 2459.7(1) Å^3.[28] Its structure, solved ab initio from synchrotron powder diffraction data, contains 17 non-hydrogen atoms in the asymmetric part of the unit cell: one Mg^{2+} ion, located in a special position, one H_6ODTMP^{2-} ligand, and one crystallographically independent water molecule. The one-half dimethylformamide molecule could not be located and is likely disordered within the structure. The Mg^{2+} ions are surrounded by six O atoms from hydrogenphosphonate groups, giving a slightly distorted octahedral environment with bond distances ranging between 2.03 and 2.16 Å, see Figure 4. The ligand
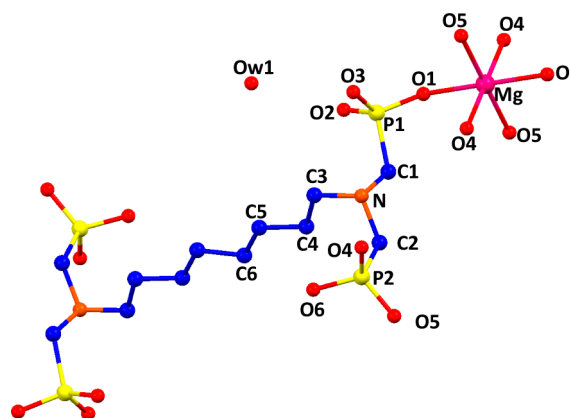

Figure 4. Selected ball−stick view for **1** with atoms labeled showing the octahedral environment of magnesium.

molecule is likely in a zwitterionic form, with the negative charges located on monodeprotonated phosphonate groups and the positive charges on the N atoms, as found in previous works.[13−15] Although the hydrogens could not be located in this work and single-crystal data are needed to definitively settle this point, the presence in the IR spectrum of several superimposed bands of medium intensity in the range 2600−2200 cm^{-1}, which can be referred to the $R_3N−H^+$ vibrations,[29] could support this assumption. There are two crystallographically independent phosphorus atoms. P1 is bonded to Mg^{2+} through only one oxygen atom, and the remaining two phosphonate oxygens are noncoordinating. P2 bridges two Mg^{2+} through two oxygen atoms, whereas the third oxygen atom is uncoordinated and points out of the plane, see Figure 4. The inorganic layer is built in the bc plane by MgO_6 octahedra arranged in square polygonal fashion, see Figure S3, Supporting Information. The Mg^{2+} ions located in the corners of each square polygon are interconnected by two amino-bis-(methylenephosphonate) moieties and two P2 phosphonate groups corresponding to four different ligands, forming one central 16-membered ring and two 12-membered rings, see Figure S3, Supporting Information. Neighboring layers are connected along the a axis by the organic groups
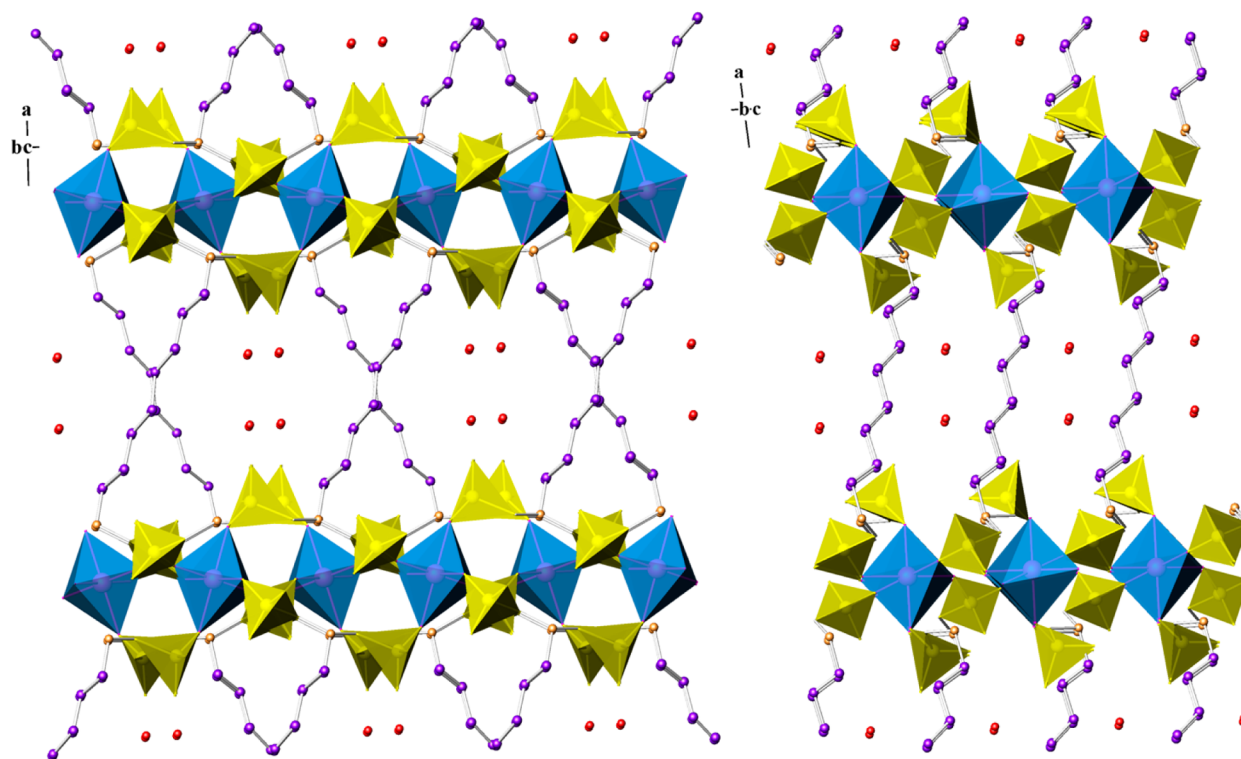
Figure 5. Crystal structure views for **1**. Framework constructed as MgO_6 and PO_4 polyhedra plus ball and stick for the organic ligand, with lattice water molecules shown as red spheres. DMF molecules not shown as they were not located. (a) View along the *c* axis (*a* axis vertical). (b) View along the *b* axis (*a* axis vertical).

$-(CH_2)_2NH-(CH_2)_8-NH-(CH_2)_2-$ in cross-diagonal fashion. This linkage results in an open 3D pillared framework, with two types of 1D channels filled by water and remnant DMF molecules, see Figure 5. The channels running along the *c* axis are wider that those running along the *b* axis, see Figure 5. The water molecules are situated close to the center of the channels interacting with each other by H bonds, O···O interacting distance of 2.75 Å, and with an oxygen of a POH group, O···O interacting distance of 2.79 Å.

The crystal structure of **1** resembles that of La-$(H_5HDTMP)\cdot7H_2O$,[15] but both differ in the way the layer and the 1D channels are built. The 8-membered rings connecting pairs of metal ions in the layers of La-$(H_5HDTMP)\cdot7H_2O$ are replaced by 12-membered rings in MgH_6ODTMP. Thus, the chains of MO_6 polyhedra, doubly bridged by phosphonate groups in LaH_5DTMP, appear bridged by only one hydrogenphosphonate group, P2, in the layer of **1**. These structural variations give rise to corrugated layers in LaH_5DTMP, while planar layers are formed in **1**.

Other di- and trivalent diaminomethylene−tetraphosphonates displaying pillared frameworks also exhibit chains of MO_6 polyhedra with double phosphonate bridges similar to those found in LaH_5DTMP, albeit this common structural motif, present in a majority of compounds, not necessarily results in the same framework (e.g., $ZnH_6HDTMP\cdot H_2O$).[13d,30] A different way of connecting the metal to the tetraphosphonate ligand lead to 2D architecture.[14] In this case, each amino-bis(methylenephosphonate) moiety chelates to a M^{2+} ion through the two phosphonate groups and the whole ligand H_6HDTMP bridges two M^{2+} ions. These units are connected to each other through bridge oxygens of phosphonate groups extending into a layered structure, e.g., $CaH_6HDTMP\cdot2H_2O$.[14] In contrast, the 3D frameworks are characterized by having two

metal centers coordinated to one amino-bis-(methylenephosphonate) moiety, which forces the organic linker to connect the inorganic layers defined by the interaction of the metal ion with the phosphonate groups. It is noteworthy that despite the variations in connectivity and metal charge the metal diaminotetraphosphonates keep the same stoichiometry, i.e., a metal:ligand ratio 1:1, that is reached by fine tuning of the protonation degree on the phosphonate terminal groups.

Gas Adsorption Characterization. N_2, CO_2, and CH_4 adsorption isotherms were measured for degassed **1**, MgH_6ODTMP, as indicated in the Experimental Section. N_2 adsorption was very low, giving a specific surface of 4 $m^2\cdot g^{-1}$. On the other hand, the CO_2 adsorption isotherm (see Figure S4, Supporting Information), collected at 273 K and under pressure up to 1 bar, gave a surface area of 180 $m^2\cdot g^{-1}$, deduced from the Dubinin−Radushkevich[24] equation and an adsorption capacity of 0.8 $mmol\cdot g^{-1}$. This clearly indicates that there are severe diffusional limitations for N_2 adsorption at 77 K in MgH_6ODTMP material and therefore could be useful for CO_2/N_2 separation. Similar values have been reported for Mg-MOF-1, constructed by helical assembly of Mg^{2+} ions with achiral 3,5-pyridine dicarboxylates,[5] but are considerably lower than those obtained for Mg/DOBDC (DOBDC = dioxybenzenedicarbox-ylate) (8 $mmol\cdot g^{-1}$ at 1 bar and 296 K), the highest adsorption capacity to date among the Mg−MOFs materials.[3i,j] The high CO_2 uptake in the latter has been associated with the ability to generate coordinatively unsaturated metal sites upon evacuation. Such modification is not possible for MgH_6ODTMP where the coordination sphere of the Mg^{2+} ion is entirely occupied by phosphonate oxygen atoms and thus cannot be upon evacuation.

Isosteric heats of adsorption, q_{st}, for carbon dioxide and methane on MgH_6ODTMP were derived from a Virial-type

expression fitted to the adsorption isotherms measured at 273, 283, 293, 303, and 318 K and calculated applying the Clausius–Clapeyron equation. The isosteric heat of CO_2 at different coverages is around 26 kJ mol^{-1} (Figure S5, Supporting Information), consistent with the presence of weak adsorption sites and showing that there are no preferential sites for CO_2 adsorption in the MgH_6ODTMP structure, as the most favorable sites for the CO_2 molecules are occupied first within a relatively rigid structure.[31] The q_{st} for CH_4, Figure S5, Supporting Information, is around 15 kJ mol^{-1}, also very similar to values previously reported for other MOFs.[32]

The CO_2/CH_4 selectivity of MgH_6ODTMP calculated from the pure gas adsorption isotherms exhibits a maximum at low coverages close to 14 that slowly decreases as the pressure increases (see Figure S6, Supporting Information). Notoriously, the selectivity observed on MgH_6ODTMP is always above 3, which is taken as a target value for industrial application.[33,34] However, the low adsorption capacity of the studied material suggests it cannot be used in adsorption processes but still could be of interest for membrane technologies where no high adsorption capacity is required.

CO_2 adsorption data for MgH_6ODTMP at low and high pressures at 303 K are shown in Figure 6. The CO_2 adsorption
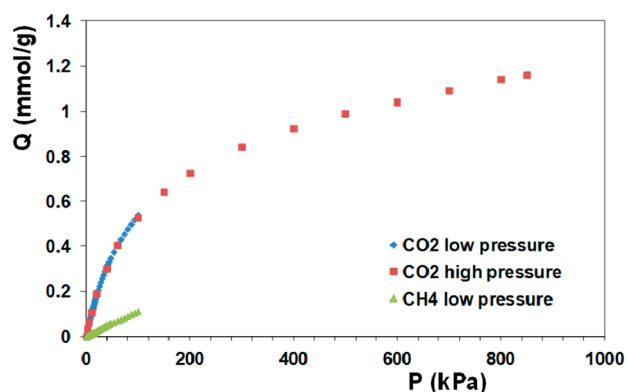

Figure 6. Adsorption isotherms for vacuum-degassed **1**. Low-pressure adsorption isotherms, up to 100 kPa, for CO_2 and CH_4. In addition, the high-pressure CO_2 isotherm up to 900 kPa is also shown.

capacity at 900 kPa is doubled with respect to that obtained at 100 kPa. This behavior suggests that the interaction of this molecule with the solid is not strong (also indicted by the low heat of adsorption), allowing easy regeneration of MgH_6ODTMP.

Proton-Conductivity Study. An ionic conductivity study has been performed using **3** ($MgH_6ODTMP·6H_2O$) as starting material. The structural study of these Mg hybrids showed 1D channels filled with water molecules running along the c and b axes (see Figure 5). These structural features, in addition to the POH groups pointing toward the channels, may allow proton conductivity to take place. Impedance spectra at different relative humidity (RH) values and temperatures are shown in Figure 7. It is worth noting that the water content within the channels, at different water partial pressures (or relative humidity), varies as shown in a previous section. At the lowest measured RH% value, depressed broad arcs are observed, which is likely due to the presence of both bulk and grain boundary contributions. At constant RH, the conductivity decreases with lowering temperature, as expected. At 90% and 94% RH development of a spike is observed, which is the main

characteristic at the highest RH% value. These spikes have associated capacitances of ~1 μF, and since they are inclined to the Z axis at ~70–80° they indicate a partial-blocking electrode response that allows limited diffusion; therefore, the conducting species must be ionic, i.e., H$^+$ ions. The total pellet resistance, R_T, is obtained from the intercept of the spike and/or the arc (low-frequency end) on the Z axis.

The small studied temperature range (282–292 K) was chosen to ensure constant water content. Thus, the conductivity variation (within this small range) only depends upon temperature, and therefore, activation energy can be derived. At higher temperatures, the compound equilibrates to a different (smaller) water content. Figure 8a displays the overall pellet conductivities, in traditional Arrhenius plots, as a function of RH. These plots show a linear behavior with apparent activation energies of 0.31, 0.59, 0.44, and 0.49 eV for RH values of 100, 94, 90, and 82, respectively. These relatively small numbers, except for RH = 94, are within the range typically attributed to a Grotthuss transfer mechanism via water molecules, 0.1–0.5 eV.[35] We speculate that the high value of apparent activation energy at RH = 94%, 0.59 eV, may be due to a lack of equilibration of the sample water content under the measured experimental conditions. Figure 8b shows a linear behavior of the proton conductivity with water partial pressure. We highlight that the reported change in the water partial pressure (from ~0.018 to ~0.022 atm) implies a 4 orders of magnitude change in the proton conductivity.

The value obtained for the proton conductivity at room temperature for $MgH_6ODTMP·6H_2O$, $\sigma = 1.6 \times 10^{-3}$ S cm^{-1} at $T = 292$ K and RH $\approx 100\%$, is higher than that recently reported for a metal phosphonate MOF material, $\sigma = 3.5 \times 10^{-5}$ S cm^{-1} at $T = 29$ 8K and RH = 98%,[9h] but slightly smaller than that of $La(H_5HDTMP)·7H_2O$, $\sigma = 8 \times 10^{-3}$ S cm^{-1} at $T = 297$ K and RH = 98%, which has an apparent activation energy of 0.25 eV.[15] Values of the same magnitude for proton conductivity, $\sigma = 1.1 \times 10^{-3}$ S cm^{-1}, at room temperature with activation energy values of 0.23 eV have been very recently reported for a carboxylate MOF.[10]

■ CONCLUSIONS

A systematic study using high-throughput methodology has allowed us to isolate a new magnesium hybrid material, $MgH_6ODTMP·2H_2O(DMF)_{0.5}$ (**1**), using as precursor the tetraphosphonic acid H_8ODTMP, octamethylenediamine-N,N,N',N'-tetrakis(methylenephosphonic acid). Its crystal structure is characterized by a novel 3D pillared open framework which contains cross-linked 1D channels filled with water and DMF. The presence of an aliphatic $-(CH_2)_8-$ chain in the ligand provides a substantial framework flexibility as the structures are adapted to the guest molecule (water) content. Thus, upon evacuation of H_2O and DMF molecules from the channels, thermally or under vacuum, the rehydration of the compound leads to a new crystalline phase with higher water content, $MgH_6ODTMP·6H_2O$ (**3**). These processes take place through crystalline–quasi-amorphous–crystalline transformation, where the integrity of the framework is maintained. A water adsorption study, at a fixed temperature of 308 K, showed that $MgH_6ODTMP·nH_2O$ reversibly equilibrates its water content as a function of the water partial pressure. The anhydrous material is ultramicroporous, and the specific surface for CO_2 adsorption is 180 m^2·g^{-1} (273 K, 1 bar) with a maximum uptake of 1.2 mmol/g at 900 kPa. MgH_6ODTMP material shows a relatively high selectivity toward CO_2
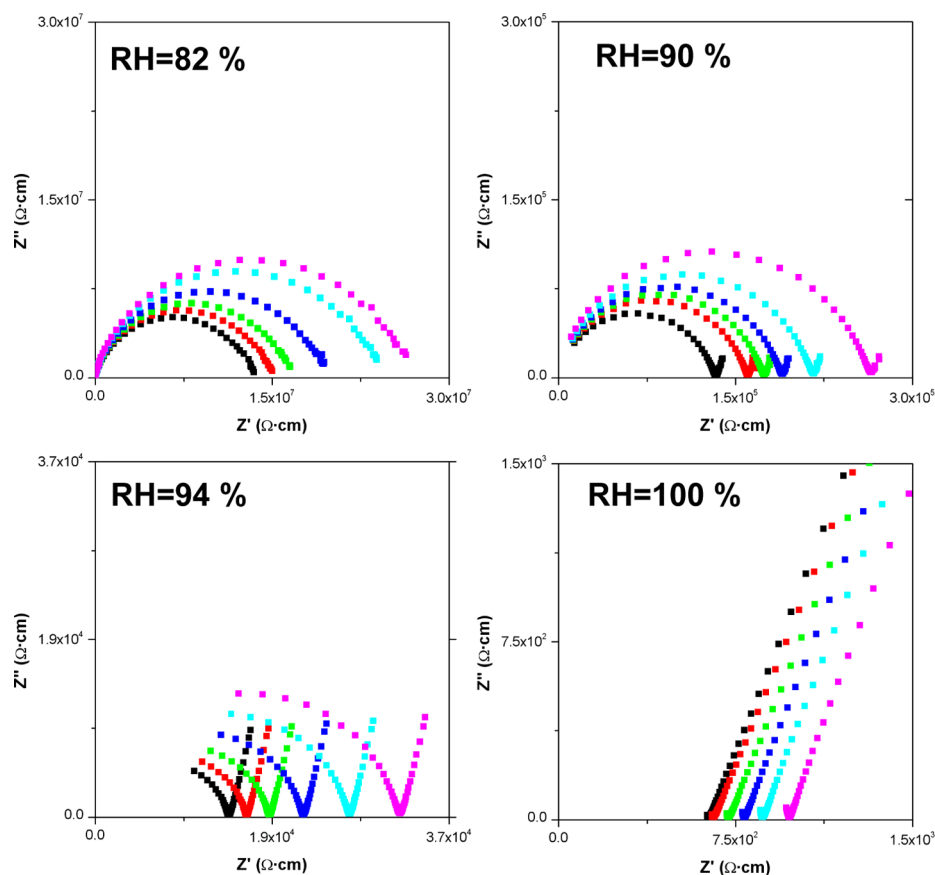
7695

dx.doi.org/10.1021/ic3007316 | *Inorg. Chem.* 2012, 51, 7689–7698

Figure 7. Plot of the complex impedance plane for $MgH_6ODTMP \cdot nH_2O$ at four relative humidities (see Experimental Section) and six temperatures: 292 (black), 290 (red), 288 (green), 286 (blue), 284 (cyan), and 282 (magenta) K. **3** was used as starting sample.
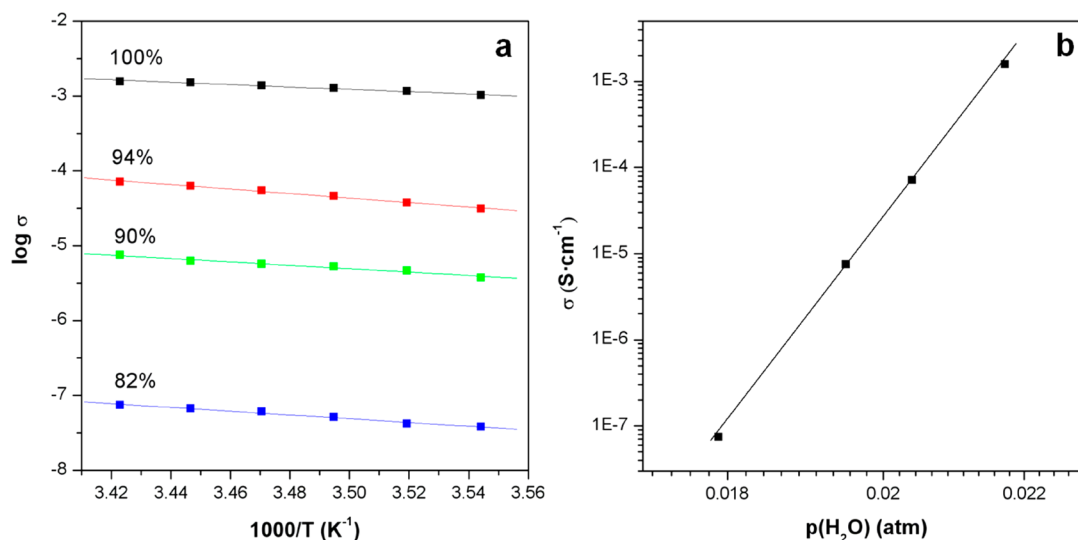

Figure 8. (a) Arrhenius plots of log σ_T for $MgH_6ODTMP \cdot nH_2O$ at four relative humidities; **3** was used as starting sample. (b) Total conductivity versus water partial pressure for $MgH_6ODTMP \cdot nH_2O$ at 19 °C in a double-logarithmic scale.

adsorption in CO_2/CH_4 mixtures and low heat of adsorption for CO_2 uptake. These findings indicate that it could be useful for natural gas upgrading. Unfortunately, its relatively low adsorption capacity makes this material inappropriate for adsorption processes and suggests that the interactions of the tested gases with the solid are not strong enough to rebuild the pillared open framework as happens with the water molecules. Finally, compound **3** shows a high proton conductivity, $\sigma = 1.6$

$\times 10^{-3}$ S cm^{-1} at $T = 292$ K at ~100% relative humidity, with an activation energy of 0.31 eV that can be attributed to a Grotthuss transfer mechanism via water molecules.

■ ASSOCIATED CONTENT

ⓢ Supporting Information
CIF file for **1**, XRPD Rietveld plot for **1**, TGA evolution for **3** under water-saturated N_2 flow, ball and stick view of a layer of

1, CO_2 and CH_4 isotherms for degassed **1**, isosteric heats of adsorption, q_{st}, for CO_2 and CH_4, CO_2/CH_4 selectivity adsorption data. This material is available free of charge via the Internet at http://pubs.acs.org.

AUTHOR INFORMATION

Corresponding Author

*E-mail: aurelio@uma.es.

Notes

The authors declare no competing financial interest.

ACKNOWLEDGMENTS

REFERENCES

(1) (a) *Topics in Current Chemistry*; Schröder, M., Ed.; Springer: New York, 2010; Vol. *293*. (b) *Metal organic frameworks: Design and application*; Macgillivray, L. R., Ed.; Wiley: New York, 2010. (c) Jiang, H.-L.; Xu, Q. *Chem. Commun.* **2011**, *47*, 3351.

(2) (a) Wharmby, M. T.; Mowat, J. P. S.; Thompson, S. P.; Wright, P. A. *J. Am. Chem. Soc.* **2011**, *133*, 1266. (b) Clegg, J. K.; Iremonger, S. S.; Hayter, M. J.; Southon, P. D.; Macquart, R. B.; Duriska, M. B.; Jensen, P.; Turner, P.; Jolliffe, K. A.; Kepert, C. J.; Meehan, G. V.; Lindoy, L. F. *Angew. Chem., Int. Ed.* **2010**, *49*, 1075.

(3) (a) Britt, D.; Furukawa, H.; Wang, B.; Yaghi, O. M. *Proc. Natl. Acad. Sci. U.S.A.* **2009**, *106*, 20637. (b) Bao, Z.; Yu, L.; Ren, Q.; Lu, X.; Deng, S. *J. Colloid Interface Sci.* **2011**, *353*, 549. (c) Glover, T. G.; Peterson, G. W.; Schindler, B. J.; Britt, D.; Yaghi, O. M. *Chem. Eng. Sci.* **2011**, *66*, 163. (d) *Hybrid Materials: Strategies, Syntheses, Characterization and Applications*; Kickelbick, G., Ed.; Wiley-VCH: Weinheim, 2007. (e) Liu, D.; Zhong, C. *J. Mater. Chem.* **2010**, *20*, 10308. (f) Ma, S.; Zhou, H.-C. *Chem. Commun.* **2010**, *46*, 44. (g) Li, J.-R.; Kuppler, R. J.; Zhou, H.-C. *Chem. Soc. Rev.* **2009**, *38*, 1477. (h) Hao, G. P.; Li, W.-C.; Lu, A.-H. *J. Mater. Chem.* **2011**, *21*, 6447. (i) Caskey, S. R.; Wong-Foy, A. G.; Matzger, A. J. *J. Am. Chem. Soc.* **2008**, *130*, 10870. (j) Mason, J. A.; Sumida, K.; Herm, Z. R.; Krishna, R.; Long, J. R. *Energy Environ. Sci.* **2011**, *4*, 3030.

(4) (a) Ferey, G.; Serre, C.; Devic, T.; Maurin, G.; Jobic, H.; Llewellyn, P. L.; Weireld, G. D.; Vimont, A.; Daturi, M.; Chang, J.-S. *Chem. Soc. Rev.* **2011**, *40*, 550. (b) Hao, G.-P.; Li, W.-C.; Lu, A.-H. *J. Mater. Chem.* **2011**, *21*, 6447. (c) Bureekaew, S.; Shimomura, S.; Kitagawa, S. *Sci. Technol. Adv. Mater.* **2008**, *9*, 014108.

(5) Mallick, A.; Saha, S.; Pachfule, P.; Roy, S.; Banerjee, R. *J. Mater. Chem.* **2010**, *20*, 9073.

(6) Bohnsack, A. M.; Ibarra, I. A.; Hatfield, P. W.; Yoon, J. W.; Hwang, Y. K.; Chang, J.-S.; Humphrey, S. M. *Chem. Commun.* **2011**, *47*, 4899.

(7) (a) Han, S. S.; Deng, W.-Q.; Goddard, W. A. *Angew. Chem., Int. Ed.* **2007**, *46*, 6289. (b) Thornton, A. W.; Nairn, K. M.; Hill, J. M.; Hill, A. J.; Hill, M. R. *J. Am. Chem. Soc.* **2009**, *131*, 10662. (c) Volkringer, C.; Loiseau, T.; Marrot, J.; Ferey, G. *CrystEngComm* **2009**, *11*, 58. (d) Cheon, Y. E.; Park, J.; Suh, M. P. *Chem. Commun.* **2009**, 5436. (e) Zhou, W.; Wu, H.; Yildirim, T. *J. Am. Chem. Soc.* **2008**, *130*, 15268. (f) Davies, R. P.; Less, R. J.; Lickiss, P. D.; White, A. J. P. *Dalton Trans.* **2007**, 2528. (g) Dinca, M.; Long, J. R. *J. Am. Chem. Soc.* **2005**, *127*, 9376.

(8) Sahoo, S. C.; Kundu, T.; Banerjee, R. *J. Am. Chem. Soc.* **2011**, *133*, 17950.

(9) (a) Jeong, N. C.; Samanta, B.; Lee, C. Y.; Farha, O. K.; Hupp, J. T. *J. Am. Chem. Soc.* **2012**, *134*, 51. (b) Bureekaew, S.; Horike, S.; Higuchi, M.; Mizuno, M.; Kawamura, T.; Tanaka, D.; Yanai, N.; Kitagawa, S. *Nat. Mater.* **2009**, *8*, 831. (c) Sadakiyo, M.; Yamada, T.; Kitagawa, H. *J. Am. Chem. Soc.* **2009**, *131*, 9906. (d) Yamada, T.; Sadakiyo, M.; Kitagawa, H. *J. Am. Chem. Soc.* **2009**, *131*, 3144. (e) Shigematsu, A.; Yamada, T.; Kitagawa, H. *J. Am. Chem. Soc.* **2011**, *133*, 2144. (f) Morikawa, S.; Yamada, T.; Kitagawa, H. *Chem. Lett.* **2009**, *38*, 654. (g) Shigematsu, A.; Yamada, T.; Kitagawa, H. *J. Am. Chem. Soc.* **2011**, *133*, 2034. (h) Taylor, J. M.; Mah, R. K.; Moudrakovski, I. L.; Ratcliffe, C. I.; Vaidhyanathan, R.; Shimizu, G. K. H. *J. Am. Chem. Soc.* **2010**, *132*, 14055.

(10) Pardo, E.; Train, C.; Gontard, G.; Boubekeur, K.; Fabelo, O.; Liu, H.; Dkhil, B.; Lloret, F.; Nakagawa, K.; Tokoro, H.; Ohkoshi, S.; Verdaguer, M. *J. Am. Chem. Soc.* **2011**, *133*, 15328.

(11) (a) *Metal Phosphonate Chemistry: From Synthesis to Applications*; Clearfield, A., Demadis, K. D., Eds.; RSC Publishing: Cambridge, 2012. (b) Gagnon, K. J.; Perry, H. P.; Clearfield, A. *Chem. Rev.* **2012**, *112*, 1034. (c) Clearfield, A. *Dalton Trans.* **2008**, *44*, 6089.

(12) (a) S. Kirumakki, S.; Huang, J.; Subbiah, A.; Yao, J.; Rowland, A.; Smith, B.; Mukherjee, A.; Samarajeewa, S.; Clearfield, A. *J. Mater. Chem.* **2009**, *19*, 2593. (b) Gomez-Alcantara, M. M.; Cabeza, A.; Moreno-Real, L.; Aranda, M. A. G.; Clearfield, A. *Microporous Mesoporous Mater.* **2006**, *88*, 293. (c) Gómez-Alcántara, M. M.; Cabeza, A.; Olivera-Pastor, P.; Fernández-Moreno, F.; Sobrados, I.; Sanz, J.; Morris, R. E.; Clearfield, A.; Aranda, M. A. G. *Dalton Trans.* **2007**, 2394. (d) Brunet, E.; Alhendawi, H. M. H.; Cerro, C.; de la Mata, M. J.; Juanes, O.; Rodríguez-Ubis, J. C. *Angew. Chem., Int. Ed.* **2006**, *45*, 6918. (e) Cabeza, A.; Gomez-Alcantara, M. M.; Olivera-Pastor, P.; Sobrados, I.; Sanz, J.; Xiao, B.; Morris, R. E.; Clearfield, A.; Aranda, M. A. G. *Microporous Mesoporous Mater.* **2008**, *114*, 322.

(13) (a) Plabst, M.; McCusker, L. B; Bein, T. *J. Am. Chem. Soc.* **2009**, *131*, 18112. (b) Costantino, F.; Ienco, A.; Gentili, P. L.; Presciutti, F. *Cryst. Growth Des.* **2010**, *10*, 4831. (c) Stock, N.; Rauscher, M.; Bein, T. *J. Solid State Chem.* **2004**, *177*, 642. (d) Demadis, K. D.; Mantzaridis, C.; Raptis, R. G.; Mezei, G. *Inorg. Chem.* **2005**, *44*, 4469. (e) Demadis, K. D.; Barouda, E.; Stavgianoudaki, N.; Zhao, H. *Cryst. Growth Des.* **2009**, *9*, 1250. (f) Demadis, K. D.; Barouda, E.; Zhao, H.; Raptis, R. G. *Polyhedron* **2009**, *28*, 3361. (g) Mondry, A.; Janicki, R. *Dalton Trans.* **2006**, 4702. (h) Wu, J.; Hou, H.; Han, H.; Fan, Y. *Inorg. Chem.* **2007**, *46*, 7960. (i) Demadis, K. D.; Barouda, E.; Raptis, R. G.; Zhao, H. *Inorg. Chem.* **2009**, *48*, 819. (j) Demadis, K. D.; Mantzaridis, C.; Lykoudis, P. *Ind. Eng. Chem. Res.* **2006**, *45*, 7795. (k) Akyol, E.; Öner, M.; Barouda, E.; Demadis, K. D. *Cryst. Growth Des.* **2009**, *9*, 5145.

(14) Colodrero, R. M. P.; Cabeza, A.; Olivera-Pastor, P.; Infantes-Molina, A.; Barouda, E.; Demadis, K. D.; Aranda, M. A. G. *Chem.—Eur. J.* **2009**, *15*, 6612.

(15) Colodrero, R. M. P.; Olivera-Pastor, P.; Losilla, E. R.; Aranda, M. A. G.; Leon-Reina, L.; Papadaki, M.; McKinlay, A. C.; Morris, R. E.; Demadis, K. D.; Cabeza, A. *Dalton Trans.* **2012**, *41*, 4045.

(16) Villemin, D.; Moreau, B.; Elbilali, A.; Didi, M.-A.; Kaid, M.; Jaffrès, P.-A. *Phosphorus Sulfur Silicon* **2010**, *185*, 2511.

(17) Colodrero, R. M. P.; Olivera-Pastor, P.; Cabeza, A.; Papadaki, M.; Demadis, K. D.; Aranda, M. A. G. *Inorg. Chem.* **2010**, *49*, 761.

(18) Boultif, A.; Louer, D. *J. Appl. Crystallogr.* **2004**, *37*, 724.

(19) Rius, J.; Vallcorba, O.; Peral, I.; Frontera, C.; Miravitlles, C. DAjust Software. Pattern matching, space group determination and intesity extraction from powder diffraction data; Instituto de Ciencias de los Materiales de Barcelona (CSIC), Spain, 2011.

(20) Rius, J. *Acta Crystallogr.* **2011**, *A67*, 63.

(21) Rietveld, H. M. *J. Appl. Crystallogr.* **1969**, *2*, 65.

(22) Larson A. C. Von Dreele, R. B. General Structure Analysis System (GSAS); Los Alamos National Laboratory Report LAUR 86-748, 2004.

(23) Toby, B. H. *J. Appl. Crystallogr.* **2001**, *34*, 210.

(24) Dubinin, M.; Radushkevich, L. V. *Proc. Acad. Sci. U.S.S.R.* **1947**, *55*, 331.

(25) Talu, O.; Li, J.; Kumar, R.; Mathias, P. M.; Moyer, J. D.; Schork, J. *Gas Sep. Purif.* **1996**, *10*, 149.

(26) Hill, T. L. *J. Chem. Phys.* **1949**, *17*, 520.

(27) *winDETA*; Novocontrol GmbH: Hundsangen, Germany, 1995.

(28) Crystal data for **1**: $a = 29.5527(9)$ Å, $b = 8.6176(2)$ Å, $c = 9.7032(2)$ Å, $\beta = 95.441(2)°$, $V = 2460.0(1)$ Å^3, $\lambda = 0.2998$ Å, $T = 293$ K, $C2/c$ space group, $Z = 4$, 1027 independent reflections, data/restrains/parameters = 7184/35/101, $R_{WP} = 0.0671$, $R_P = 0.0495$, $R_F = 0.0734$, CCDC number 815762.

(29) Socrates, G. *Infrared and Raman Characteristic Group Frequencies: Tables and Charts*; John Wiley & Sons: Chichester, 2001.

(30) (a) Stock, N.; Stoll, A.; Bein, T. *Microporous Mesoporous Mater.* **2004**, *69*, 65. (b) Stock, N.; Rauscher, M.; Bein, T. *J. Solid State Chem.* **2004**, *177*, 642. (c) Stock, N.; Bein, T. *Angew. Chem., Int. Ed.* **2004**, *43*, 749.

(31) Stylianou, K. C.; Warren, J. E.; Chong, S. Y.; Rabone, J.; Bacsa, J.; Bradshaw, D.; Rosseinsky, M. J. *Chem. Commun.* **2011**, *47*, 3389.

(32) Bhatia, S. K.; Myers., A. L. *Langmuir* **2006**, *22*, 1688.

(33) Delgado, J. A.; Uguina, M. A.; Gomez, J. M.; Ortega, L. *Separ. Purif. Technol.* **2006**, *48*, 223.

(34) Palomino, M.; Corma, A.; Rey, F.; Valencia, S. *Langmuir* **2010**, *26*, 1910.

(35) Colomban, P. Proton Conductors: Solids, Membranes and Gels Materials and Devices. *Chemistry of Solid State Materials*; Cambridge University Press: Cambridge, U.K., 1992; Vol. 2.